Palomar adaptive optics project: status and performance

M. Troy[a], R. Dekany[a], G. Brack[a], B. Oppenheimer[b], E. Bloemhof[c],
T. Trinh[a], F. Dekens[a], F. Shi[a], T. Hayward[d*], and B. Brandl[d]

[a]Jet Propulsion Laboratory, California Institute of Technology, Pasadena, CA, USA 91109

[b]Astronomy Dept., University of California Berkeley, CA, USA 94720

[c]Palomar Observatory, California Institute of Technology, Pasadena, CA, USA 91125

[d]Astronomy Dept., Cornell University Ithaca, NY, USA 14853

ABSTRACT

We describe the current performance of the Palomar 200 inch (5 m) adaptive optics system, which in December of 1998 achieved its first high order (241 actuators) lock on a natural guide star. In the K band (2.2 μm), the system has achieved Strehl ratios as high as 50% in the presence of 1.0 arcsecond seeing (0.5 μm). Predictions of the system's performance based on the analysis of real-time wavefront sensor telemetry data and a analysis based on a fitted Kolmogorov atmospheric model are shown to both agree with the observed science image performance. Performance predictions for various seeing conditions are presented and an analysis of the error budget is used to show which subsystems limit the performance of the AO system under various atmospheric conditions.

Keywords: Adaptive optics, telescopes, instrumentation, atmospheric characterization

1. INTRODUCTION

The Palomar Adaptive Optics system (PALAO) is a facility adaptive optics (AO) system for use at the f/15.7 Cassegrain focus of the Palomar 200" Hale telescope. The instrument was built and designed at the Jet Propulsion Laboratory. In March of 1998, PALAO achieved its first tip/tilt lock on a natural guide star.[1] About one year later the system achieved it's first high order lock on a natural guide star. In August of 1999 the system started shared-risk observing supporting nine groups of observers over ten nights of observing in five months. In May of 2000, PALAO will become a facility instrument available for use by any observer. The system routinely achieves Strehls of 50% (in K) on guide stars brighter then 8th magnitude in the presence of 1 arcsecond seeing (0.5 μm) with estimated wind velocities on the order of 5 to 10 m/s.

In the remainder of this paper we will analyze and predict the system performance with the use of wavefront sensor telemetry data. These results are then compared to image data obtained from the PALAO science instrument. This data is presented in section 2. Section 3 presents the analysis of the real-time telemetry data to fit atmospheric parameters, which are then used later to predict the system performance. In section 4, we analyze the system performance (in terms of science Strehl ratio) as a sum of individual error terms. We estimate the individual error terms, both from the fitted atmospheric model and by analyzing telemetry data, from PALAO observations of two different objects. We then compare these performance predictions to the actual performance as measured with science images. In section 5, we present system performance predictions for various seeing conditions and guide star magnitudes. We conclude (section 6) with a discussion of the factors limiting current performance and the plans to improve them.

2. DATA

PALAO has a rather unique wavefront sensor (WFS) telemetry data recording ability. With the WFS running at 500 Hz, every 5th frame of data (or 100 Hz) can be recorded for as long as desired (or until the 70+GB of disk space is filled). The telemetry data consists of centroid positions, centroid flux, tip/tilt mirror positions and residuals, and deformable mirror (DM) positions and residuals. Raw or flat-fielded pixel data can also be recorded continuously at speeds up to 10 Hz. This telemetry data is used here to predict the system performance.

---

*Currently with Gemini Observatory, Hilo, HI 96720

The first PALAO observation we analyze is of Gamma Oph (V=3.75) on UT 99Aug29. In this case the WFS was running at 550 Hz and recording every 5th frame of data (or 110 Hz). The second observation is SAO 146421 (V=7.43), on UT 99Sep28, with the WFS running at 500 Hz and recording every 5th frame of data (or 100 Hz). Telemetry data was collected with both the deformable mirror (DM) and tip/tilt loops open and closed. The PALAO science instrument, the Palomar High Angular Resolution Observer (PHARO),[2] was used to obtain closed loop K band images. These images provide a measure of the actual Strehl ratios achieved.

3. ATMOSPHERIC PARAMETERS

The atmospheric coherence length (or Fried parameter[3]) can be obtained from the open loop centroid telemetry using the following equation[4]:

$$r_0 = d_s \left[0.4488 \left(\frac{\lambda}{2\pi} \right)^2 \left(\frac{4}{d_s} \right)^2 \left(\frac{1}{\sigma_c^2} \right) \right]^{\frac{3}{5}} [m], \tag{1}$$

where σ_c^2 is the mean-square centroid motions over a subaperture of diameter d_s. The Fried parameter, denoted as r_0, is calculated at a wavelength, λ, which is not necessarily the wavelength where the centroid motion were measured. Unless otherwise noted, r_0 is quoted at 0.5 μm. The RMS centroid motion (σ_c) can be calculated from the open loop centroid data for each of the approximately 212 active WFS subapertures, each with an effective diameter of $d_s = 35.3$ cm. We then take the average r_0 over all the subapertures. Using the subapertures, instead of the whole aperture, provides a result (nearly) independent of the outer scale of turbulence, which is expected to be much larger then the subaperture diameter.

Using 60 seconds of telemetry data to calculate σ_c and inserting into Eq. 1, we calculate an r_0 of 12 cm and 13 cm for Gamma Oph and SAO 146421 respectively. These values are equivalent to about 0.8 arcsecond seeing (λ/r_0). The wind velocity can be estimated from the break frequency of the open loop tip/tilt power spectral densities (PSD). The break occurs[4] at a frequency of $v/(4.2D)$, where v is the wind velocity. Figures 1 and 2 show the open and closed loop tip/tilt PSDs. The estimated break point is 0.25 Hz for both objects. This results in an estimated wind velocity of 5 m/s.
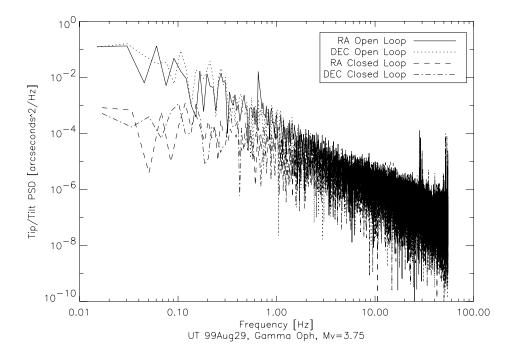

Figure 1. The open and closed loop tip/tilt PSD while observing Gamma Oph
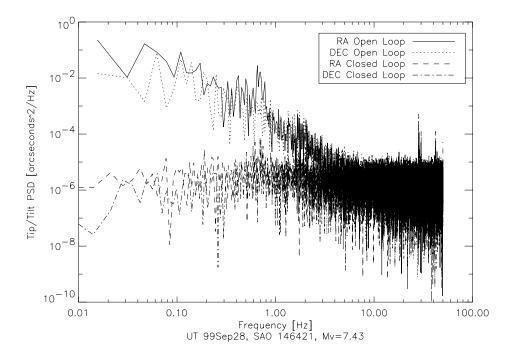
Figure 2. The open and closed loop tip/tilt PSD while observing SAO 146421

4. MEASURED ON-AXIS GUIDE STAR PERFORMANCE

The performance of an AO system can be characterized in terms of the mean-squared wavefront error (σ^2) which is a sum of individual error terms, σ_i^2. This addition of the error terms in quadrature assumes that the individual error terms, σ_i are independent. If the individual error terms are not independent then the total error will be over-estimated and the system performance under-estimated. A useful metric in quantifying an AO system performance is the Strehl ratio, which is the ratio of the measured peak intensity in the image plane divided by the peak intensity of a perfect wavefront propagated through the telescope. When the wavefront errors are less then about $\frac{\lambda}{4\pi}$ RMS meters, the Strehl ratio can be estimated by the Marechal approximation[5] $S \approx e^{-\sigma^2}$. We describe the performance of a natural guide star adaptive optics system as a sum of the following error terms:

$$\sigma_{TOTAL}^2 = \sigma_{TD}^2 + \sigma_{RT}^2 + \sigma_{AF}^2 + \sigma_{TF}^2 + \sigma_{CAL}^2 + \sigma_{WFS}^2, \tag{2}$$

where σ_{TOTAL} is the total on-axis guide star performance error, σ_{TD} is the time-delay error from the deformable mirror (DM) servo loop, σ_{RT} is the residual tip/tilt errors, σ_{AF} is the atmospheric fitting error from trying to correct the atmosphere with a given DM actuator spacing, σ_{TF} is from fitting the telescope with the DM actuator spacing, σ_{CAL} is the calibration error and σ_{WFS} is the wavefront sensor (WFS) measurement error's contribution to high order aberrations. While these are not the only error terms for an on-axis guide star they are the dominant error terms for the PALAO system.

In the remainder of this section we discuss the values for each of the above terms. Whenever possible both theoretical and empirical values are presented for each error term. The empirical values are calculated using the PALAO telemetry data for observations of the two different objects presented in section 2. The "theoretical" values use the atmospheric parameters determined in section 3 along with servo loop bandwidths estimated in subsections 4.1 and 4.2. In the final subsection (4.7), we bring all the error terms together to get both theoretical and experimental estimates of the PALAO system performance for the two cases. We compare these predicted Strehl ratios to the Strehl ratios actually obtained with the science instrument, PHARO.

4.1. Time-delay σ_{TD}

The mean-square phase error (in radians squared) resulting from the DM servo control loop and time-delay is[6]:

$$\sigma_{TD}^2 = k \left(\frac{f_G}{f_S} \right)^{5/3} [rad^2] \qquad (3)$$

where f_G is the Greenwood frequency, f_S is the servo bandwidth of the system and k ranges from 1 for a simple RC network to 0.191 for a perfect cutoff filter at frequency f_S. The PALAO servo algorithm is more like an RC filter, so we use a value of 1 for k. The Greenwood frequency may be approximated by:

$$f_G = 0.427 \frac{v}{r_0} [Hz], \qquad (4)$$

where the atmosphere is assumed to have a single turbulent layer with wind velocity v.

The closed loop DM residual errors provide an independent estimate of σ_{TD}. For a given frame of WFS data, the closed loop centroids values are multiplied by a reconstructor matrix to determine the error of each DM actuator. The RMS wavefront error is then approximately two times the RMS of these actuators values. However, one must be careful because in general the RMS of the closed loop DM residuals includes any WFS measurement noise errors. These errors should be subtracted before being compared to the atmospheric modeled value of σ_{TD}. Figure 3 is a PSD plot of the average open and closed loop DM residuals for Gamma Oph. In this case no noise floor can be seen and one can assume the contribution from WFS measurement errors is small (We will show this to be true in section 4.6). However, SAO 146421 is approximately 13 times dimmer then Gamma Oph. The PSD of the average DM residuals, shown in Figure 4, has a noise floor at approximately 5E-5 μm^2/Hz. The noise floor is assumed to be constant at all frequencies and is subtracted in quadrature from the total residual error.

From the cross-over frequency of the open and closed loop DM residuals (Figures 3 and 4) the estimated value for f_S is 15 Hz. For Gamma Oph the modeled value of σ_{TD} is 92 nm and the measured value is 57 nm. For SAO 146421 the modeled value is 86 nm and the measured value is 135 nm.

Figure 3. The power spectral density (PSD) of the open and closed loop DM residuals. The open loop DM residuals are a measure of the atmospheric phase errors. The PSDs were calculated for each DM actuator and then averaged. The servo bandwidth is about 15 Hz.
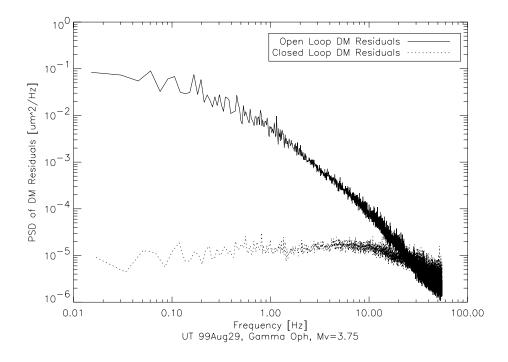
Figure 4. The power spectral density (PSD) of the open and closed loop DM residuals. The open loop DM residuals are a measure of the atmospheric phase errors. The PSDs were calculated for each DM actuator and then averaged. The servo bandwidth is about 15 Hz.
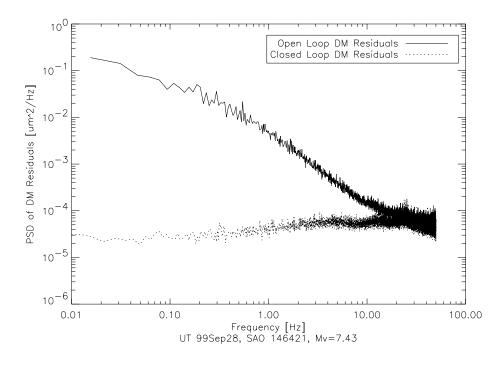
4.2. Residual Tip/Tilt Error σ_{RT}

The residual tip/tilt error (in radians) from a finite-bandwidth of an AO tip/tilt correction is given by[7]:

$$\sigma_{RT} = \left(\frac{f_T}{f_{3dB}} \right) \left(\frac{\lambda_T}{D} \right) [rad], \tag{5}$$

where f_T is the fundamental tilt tracking frequency. Assuming one layer of atmospheric turbulence at an altitude h and a zenith angle of zero, the tracking frequency can be approximated by[8]:

$$f_T \approx 0.0811 \left(\frac{r_0}{D} \right)^{1/6} \left(\frac{v(h)}{r_0} \right) [Hz] \tag{6}$$

Figures 1 and 2 showed plots of open and closed tip/tilt loop PSDs. From these we estimate the -3 dB break point of the AO tip/tilt correction to be approximately 2 Hz.

Given closed loop centroid values (from telemetry), the residual tip/tilt across the full aperture is just the RMS of the global tip/tilt values (σ_{ttcent}). These values can then be converted from radians of tip/tilt to RMS wavefront error with:

$$\sigma_{RT} = \sigma_{ttcent} \left(\frac{D}{4} \right) [m], \tag{7}$$

where $D = 5$ meters for the Palomar aperture diameter.

The empirical and modeled values of σ_{ttcent} for Gamma Oph are 0.021 and 0.018 arcseconds while those for SAO 146421 are 0.016 and 0.017 arcseconds. The empirical and modeled values in RMS wavefront are 130 and 111 nm for Gamma Oph and 100 nm and 106 nm for SAO 146421.

4.3. Atmospheric Fitting Error σ_{AF}

The atmospheric fitting error from a continuous face sheet DM is given by[9]:

$$\sigma_{AF}^2 = 0.28 \left(\frac{d_a}{r_0}\right)^{5/3} [rad^2] \tag{8}$$

were r_0 is in meters at the wavelength of interest and d_a is the spacing between actuators in the pupil plane (31.2 cm for PALAO). For an $r_0(0.5\mu m)$ of 13 cm this results in $\sigma_{AF} = 88$ nm. Note that we can not measure this directly since our WFS only samples the wavefront every d_a meters.

4.4. Telescope Fitting Error σ_{TF}

There is a fitting error for aberrations in the optical system with spatial frequency greater then the actuator spacing of the DM, which we denote as σ_{TF}. Any errors in the AO optics that can not be corrected with the DM will be included as part of the internal calibration error term (see section 4.5). So, only optics that are not measured as part of the internal calibration procedure will contribute to σ_{TF}. The optics in question are then the telescope's primary and secondary mirrors and one fold flat mirror that is used in the calibration procedure to fold the white light into the beam. Any (presumably small) aberrations from the 2 inch fold flat mirror would only serve to artificially increase the σ_{CAL} term and so is ignored in this analysis.

The telescope primary and secondary high spatial frequency errors have been estimated from curvature sensing data collected in April 1995.[10] We conservatively estimate that the DM can perfectly remove the first 25 Zernike terms. The curvature data predicts a residual RMS wavefront error of 96±19 nm, after removal of these terms. The measurement uncertainty of this term is currently not well understood and needs further investigation.

4.5. Calibration of Desired Centroid Values σ_{CAL}

Due to non-common path errors between the light reaching the WFS and that reaching the science camera, a perfect wavefront at a WFS is not a perfect wavefront on the science detector, PHARO. One must determine what wavefront at the WFS creates a perfect (or near perfect) wavefront at the science image. We call this process "image sharpening" and the associated wavefront error from this the calibration error, σ_{CAL}.

The current process for image sharpening involves locking the AO system on a white light source and looking at the image formed on PHARO. Different amounts of Zernike aberrations are added to the desired closed loop centroids values, a new PHARO image is taken, and the affects of these aberrations on the PHARO image is evaluated by "eye" to determine if the image has been improved. The first 10 Zernike terms are determined by this iterative method. This procedure takes between 15 and 30 minutes.

Currently this image sharpening procedure is carried out the first afternoon of every observing run (that is just after the AO system is mounted on the telescope) and then whenever there is a large change in night time air/dome temperature ($\gtrsim 4^0 C$) . In addition, we currently only perform the procedure on one or at most two of PHARO's filters, but the image should be sharpened, and the new desired centroid offsets calculated, for every PHARO filter (there are 12 of them) and each of the two plate scales (25 milli-arcseconds/pixel and 40 milli-arcseconds/pixel). The current method of image sharpening is too labor intensive, time consuming and (as will become apparent later) inaccurate. We are currently investigating phase diversity techniques to automate and improve the image sharpening procedure.

On September, 27 1999, the above image sharpening procedure was carried out and K band images were collected of the white light source. The Strehl was evaluated using a package developed by Marshall.[11] The K band images had a diffraction limited full width at half maximum (FWHM) and an estimated RMS wavefront error of 165 nm. This is our best estimate for the calibration error.

4.6. WFS Measurement Errors σ_{WFS}

The RMS wavefront measurement error for a Shack-Hartmann sensor is given by[12]:

$$\sigma_{WFS} \approx \frac{\pi^2 d_s}{8 r_0 SNR}[rad], \tag{9}$$

where r_0 is at the WFS sensing wavelength and the signal to noise ratio, SNR, is given by:

$$SNR = \frac{n_p}{(n_p + N_d[n_B^2 + e^2])^{(1/2)}}, \tag{10}$$

where n_p is the number of detected photon electrons in each subaperture, N_d is the number of pixels per subaperture, n_B is the number of detected background electrons, and e is the read noise in electrons (e^-). PALAO has 4 by 4 pixel subapertures so N_d is 16. For a visible wavefront sensor, n_B is essentially zero. The camera as delivered from SciMeasure read the pixels out at 1 Mpixel/sec with a read noise of about 6.0 e^-.[13] We currently read the WFS out at 2.5 Mpixels/sec (instead of 1 Mpixels/sec) in order to increase the servo bandwidths. In increasing the readout rate, however, we have increased the readout noise to about 12 e^-. It is believed this can be reduced to 7 or 8 e^- at this 2.5 Mpixels/sec rate and plans are currently underway to do so.

An additional problem is the size of the subimages formed on the WFS detector. Eq. 9 assumes that the subimages are of size λ/r_0; however, the PALAO subimages have a FWHM of approximately 1.9 arcseconds and thus are not limited in size by r_0. We use an effective r_0 of 5.5 cm to account for this.

For Gamma Oph, the SNR was 157 and for SAO 146421 it was 27. Using Eq. 9 and $r_0 = 5.5$ cm, the predicted values of σ_{WFS} are 10 and 59 nm respectively. For SAO 146421, we can use the noise floor of the DM residuals PSD to get an independent estimate of σ_{WFS}, which yields 127 nm. This discrepancy of over a factor of two is not currently understood.

4.7. Summary of on-axis terms

Table 1 shows a summary of the measured and atmospheric modeled error terms in RMS wavefront error for Gamma Oph and SAO 146421. Numbers in italics indicate that the particular term could not be determined using that method. In calculating the total error contribution, if a modeled value was not available then the measured value was used and vice-versa. The major difference between the two cases is the WFS measurement noise from the dimmer guide star (SAO 146421). In the case of the bright guide star (Gamma Oph) the modeled and measured estimates of system performance agree. The fact that the values agree exactly is just coincidental. For the dimmer guide star, the values differ by only 15%. Thus, for these two cases the telemetry based and theoretical based performance predictions agree.

Table 1. On-axis Telemetry Predicted Guide Star Performance

Error Term	RMS Wavefront Error [nm]					
	Gamma Oph			SAO 146421		
	Measured		Atmospheric Model	Measured		Atmospheric Model
σ_{TD}	57		90	135		86
σ_{RT}	130		111	100		106
σ_{AF}	*92*	$\Leftarrow$	92	*88*	$\Leftarrow$	88
σ_{TF}	96	$\Rightarrow$	*96*	96	$\Rightarrow$	*96*
σ_{CAL}	165	$\Rightarrow$	*165*	165	$\Rightarrow$	*165*
σ_{WFS}	*10*	$\Leftarrow$	10	127		59
σ_{TOTAL}	255		255	298		257

We can convert these predicted wavefront errors to Strehl ratios and compare these values directly to those obtained with PHARO images taken while the telemetry data was being recorded. Table 2 shows the K band Strehl ratios measured from PHARO images, the predicted values using telemetry and the values predicted from theory. These later two values are just the total RMS wavefront values from table 1 converted to Strehl. The Gamma Oph PHARO data consisted of twenty 0.532 second exposures taken over a period of 111 seconds. The images were analyzed using normal IR reduction techniques and then co-added. The SAO 146421 PHARO data was one 40 second exposure. In both cases the Strehl was estimated using an algorithm developed by Marshall.[11] The PALAO telemetry for these particular data sets seems to do a good job of predicting the Strehl ratio of the PHARO images.

Table 2. Comparison of Predicted and Measured Strehls

	K band Strehl Ratio		
	Measured from PHARO Image	Predicted From Telemetry	Predicted From Theory
Gamma Oph	0.60 ± 0.05	0.59	0.59
SAO 146421	0.42 ± 0.05	0.48	0.58

5. PERFORMANCE PREDICTIONS

It is useful to look at the predicted PALAO performance for various seeing conditions and guide star magnitudes in order to gain a better understanding of what is limiting the system performance. This also provides a way for observers to predict what system performance they should expect for a given seeing condition. The analysis below applies only to on-axis guide stars. For off-axis guide stars, anisoplanicity affects should also be considered.[11]

We can develop an informal estimate of typical atmospheric conditions, from the PALAO data collected during the summer of 1999. This gives an average r_0 on the order of 10 to 15 cm and an average wind speed of 5 m/s. A more quantitative study was done with 151 measurements of r_0 on 5 nights between August and October 1996 using the Palomar Alignment Camera.[4] The measured value of r_0 was 16.3 ± 5.9 cm and an average wind velocity of about 4.2 m/s. So, we take the average summer atmospheric conditions at Palomar to be a r_0 on the order of 15 cm and a wind velocity of 5 m/s. In excellent conditions r_0 may increase to as high as 25 cm.

Table 3 shows the predicted system performance in terms of RMS wavefront error and Strehl ratios for various values of r_0 and wind velocities. The seeing conditions degrade left to right in the table. Wavefront measurement noise has not been included in this table. Under excellent seeing conditions, the system can achieve Strehl ratios greater then 0.65. With wind speeds of 5 m/s and seeing of 1 arcsecond or better the system is limited by calibration error. At an r_0 of 7 cm (1.5 arcsecond seeing) all of the error terms are about equal and a Strehl of 0.4 is achieved. As the wind speed increases, the tip/tilt residual term (σ_{RT}) quickly dominates the error budget.

Table 3. Predicted On-axis Guide Star Performance

Atmospheric	r_0 [cm @ 0.5 μm]	7	7	10	10	15	20
	Wind speed [m/s]	10	5	10	5	5	5
Condition	Seeing [arcseconds @ 0.5 μm]	1.5	1.5	1.0	1.0	0.69	0.52
	σ_{TD} [nm]	256	144	190	107	76	60
Error	σ_{RT} [nm]	355	178	264	132	94	74
	σ_{AF} [nm]	146	146	108	109	78	61
Terms	σ_{TF} [nm]	96	96	96	96	96	96
	σ_{CAL} [nm]	165	165	165	165	165	165
	σ_{TOTAL}	500	332	393	277	239	222
Predicted	Strehl Ratio @ 2.20 μm	0.13	0.41	0.28	0.53	0.63	0.67
	Strehl Ratio @ 1.65 μm	0.03	0.20	0.11	0.33	0.44	0.49
Performance	Strehl Ratio @ 1.25 μm	0	0.06	0.02	0.14	0.24	0.29

Figure 5 shows the theoretical RMS wavefront error from wavefront measurement noise as a function of guide star magnitude. The solid line is the theoretical performance of the current system. The one measured data point (at mV=7.43,σ_{WFS} = 127 nm) indicates that the actual performance may be worse. We plan to investigate this in future engineering runs. At a guide star magnitude of about mV=8 the measurement error (100 nm) has little affect on the AO system performance. However, at a guide star magnitude of 9.2, the wavefront error is 250 nm or a contribution to the Strehl of 0.6. That is, with an r_0 of 10 cm and v of 5 m/s, then (using Table 3) the Strehl at K would be 0.53*0.6 or 0.3. In practice, when the σ_{WFS} errors starts to dominate the error budget, the WFS

should be slowed down to decrease the measurement error. As an example at 100 Hz, the SNR will increase by a factor of 5, thus increasing the 9.2 magnitude limit to 11.2. However, as the system is slowed down the closed loop bandwidths will decrease and σ_{TD} and σ_{RT} will increase. In principle, while operating the AO system one should optimize σ_{WFS} against servo bandwidths.

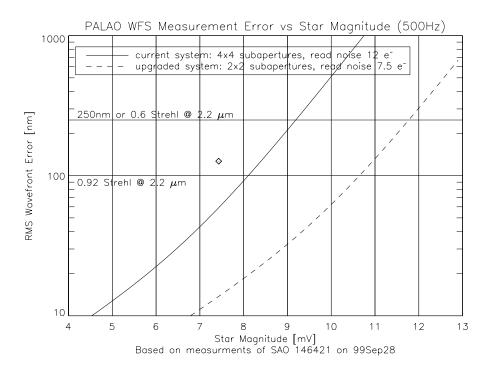PALAO WFS Measurement Error vs Star Magnitude (500Hz)

Figure 5. The WFS measurement noise (using Eq. 9) as a function of guide star magnitude. The solid line is the theoretical curve for the current system and the dashed line (which assumes an r_0 of 15 cm) is that for a planned upgrade to a new wavefront sensor.[14] The data point at mV=7.43 and $\sigma_{WFS} = 127$ nm is the measured value.

6. DISCUSSION AND FUTURE WORK

In many cases the dominant error term is that from calibration (or image sharpening). We are currently investigating using phase-diversity techniques to automate and improve this procedure. On guide stars dimmer then 7th or 8th magnitude, the WFS measurement noise (σ_{WFS}) is often a dominant error term. Within the next two years a new WFS camera[14] and new WFS optics will be implemented. The dashed line on Figure 5 indicates the expected performance. In the near term (within the next several months), we plan to reduce the read noise of the current WFS. At wind speeds greater then 10 m/s, the residual tip/tilt σ_{RT} error dominates the error budget. This is as a result of the 2 Hz closed loop bandwidth of the tip/tilt loop. Plans are underway to understand and improve this bandwidth.

We have provided estimates of the AO system performance as a function of seeing parameters (r_0 and v), and guide star magnitude. We have identified which subsystems of the AO system are limiting performance under different operating conditions. Perhaps most importantly, we have shown that the WFS telemetry data can be used to measure the various AO error terms and correctly predict the overall system performance (science Strehl). In it's most simplistic state, this type of analysis can be used in real time to understand when a subsystem is performing below expectations and predict science Strehl. Although not yet implemented, real-time analysis of the telemetry data could be used to optimized the system performance by determining the correct WFS rates and servo loop gains. Additionally, future applications of the telemetry data should include science PSF estimation.

ACKNOWLEDGMENTS

REFERENCES

1. R. G. Dekany, G. Brack, D. Palmer, B. R. Oppenheimer, T. L. Hayward, , and B. Brandl, "First tip-tilt correction with the Palomar 200-in adaptive optics system," in *Adaptive Optical System Technologies*, D. Bonnaccini and R. K. Tyson, eds., vol. 3353, pp. 56–59, SPIE, 1998.

2. B. Brandl, T. Hayward, J. Houck, G. Gull, B. Pirger, and J. Schoenwald, "PHARO (Palomar high angular resolution observer) a dedicated NIR camera for the Palomar adaptive optics system," in *Adaptive Optics and Applications*, R. K. Tyson and R. Q. Fugate, eds., vol. 3126, pp. 515–521, SPIE, 1997.

3. D. L. Fried, "Statistics of a geometric representation of wavefront distortion," *J. Opt. Soc. Am.* **55**, pp. 1427–1435, Nov. 1965.

4. F. Dekens, *Atmospheric characterization for adaptive optics at the W. M. Keck and Hale Telescopes.* PhD thesis, University of California, Irvine, Jan. 1998.

5. J. H. Hardy, *Adaptive Optics for Astronomical Telescopes*, pp. 114–115. Oxford University Press, New York, 1st ed., 1998.

6. J. H. Hardy, *Adaptive Optics for Astronomical Telescopes*, pp. 337–338. Oxford University Press, New York, 1st ed., 1998.

7. G. A. Tyer Report TR-887, The Optical Sciences Co., 1988.

8. G. Chanan, G. Djorgovski, A. Gleckler, S. Kulkarni, T. Mast, C. Max, J. Nelson, and P. Wizinowich, "*Adaptive Optics for Keck Observatory,*" Keck Observatory Report No. 208, W.M. Keck Observatory, Kamuela HI, Jan. 1996.

9. J. H. Hardy, *Adaptive Optics for Astronomical Telescopes*, pp. 342–343. Oxford University Press, New York, 1st ed., 1998.

10. R. Dekany, M. Shao, K. Wallace, D. Redding, G. Brack, B. Thicksten, H. Petrie, and M. Colavita, "Palomar 5 m adaptive optics project," critical design review, Jet Propulsion Laboratory, Pasadena CA, Nov. 1995.

11. J. Marshall, M. Troy, and R. Dekany, "Anisoplanicity studies within NGC6871," in Wizinowich.[15]

12. J. H. Hardy, *Adaptive Optics for Astronomical Telescopes*, pp. 147–150. Oxford University Press, New York, 1st ed., 1998.

13. R. DuVarney, C. Bleau, G. Motter, R. Dekany, M. Troy, and G. Brack, "SciMeasure wavefront sensor cameras and their application in the Palomar adaptive optics system," in *Proceedings of the 4th ESO workshop on Optical Detectors in Astronomy*, K. A. Publishing, ed., ESO, 1999.

14. R. DuVarney, C. Bleau, G. Motter, S. Shaklan, A. Kuhnert, G. Brack, D. Palmar, M. Troy, T. Kieu, and R. Dekany, "EEV CCD39 wavefront sensor cameras for AO and interferometry," in Wizinowich.[15]

15. P. Wizinowich, ed., *Adaptive Optical System Technologies*, vol. 4007, SPIE, 2000.